Sensor Applications

UWB bistatic radar sensor: across channels evaluation

Luca Santoro[1], Matteo Nardello[1], Daniele Fontanelli[1], Davide Brunelli[1]

[1]*Department of Industrial Engineering, Via Sommarive 9, 38123, Trento, Italy*
e-mail:name.surname@unitn.it

Manuscript received June 7, 2017; revised June 21, 2017; accepted July 6, 2017. Date of publication July 12, 2017; date of current version July 12, 2017.

Abstract—Device-Free localization is a promising technique for indoor positioning in infrastructures, as it eliminates the reliance on custom and costly hardware. In this study, we present the development of a compact and cost-effective bistatic radar sensor that utilizes DW3000 UWB transceivers. The effectiveness of the sensor was evaluated through comprehensive assessments of various channels, with particular emphasis on channel 9, employing Channel Impulse Response analysis. To enhance the accuracy of time delay estimation for multipath components scattered by moving targets, we developed a weighting function. The experimental results demonstrate the potential of device-free localization sensors as a viable solution for indoor positioning systems, offering enhanced accessibility and cost reduction compared to traditional approaches.

Index Terms—Bistatic radar; Device-free localization; UWB.

I. INTRODUCTION

In recent years, there has been a growing emphasis on integrating positioning systems into Internet of Things (IoT) and Industrial Internet of Things (IIoT) networks, mainly sparked by the technological advancements in compact and energy-efficient devices. Positioning systems can be broadly categorized into *active* [1], [2] and *passive* systems [3]. The former systems involve entities equipped with electronic devices that exchange information with the infrastructure to estimate their positions [4], [5]. In contrast, passive positioning systems involve entities that either do not carry electronic devices (for example, in healthcare applications [6]–[8], on-body sensors may not always be practical [9], [10]) or, if they do have electronic devices, do not actively contribute to the positioning algorithm and instead act as passive listeners. An illustrative example of the latter is [11], where the target determines its position by listening to messages broadcasted from the infrastructure, resembling a traditional GPS. Passive positioning systems, however, place a significant emphasis on device-free localization (DFL) systems, which involve entities without electronic devices [12]. While camera-based solutions [13], [14] are typical examples, their computational intensity, high data rates, and privacy concerns arise due to the requirement for high-resolution images. To address these limitations, acoustic and ultrasonic systems [15], [16] typically solve such drawbacks but utilize signals with distinct propagation characteristics and frequencies whose performance is easily corrupted by environmental noise. Alternatively, RF-based DFL systems have gained prominence as they monitor the target area by measuring changes in the radio channel spectrum leveraging received signal strength indicator (RSSI), channel state information (CSI), or channel impulse responses (CIRs) that enable the detection and tracking of moving entities [17], [18]. By combining positioning and tracking systems in an IoT architecture, numerous applications have emerged in various domains, such as the RF-based DFL systems for detecting and tracking non-cooperative or unauthorized targets in different environments [19], [20]. A comprehensive assessment of different technologies for DFL systems can be found in [21].

Corresponding author: L. Santoro (e-mail: luca.santoro@unitn.it)

Within the standardized RF domain IEEE *802.15.4a*, UWB networks can provide detailed time-domain CIR that can be analyzed to identify the time location of MultiPath Components (MPCs) scattered from the targets, hence facilitating the development of DFL systems, e.g., bistatic radar on low-cost commercial-off-the-shelf (COTS) modules. An early study in this domain for monitoring and safety applications is presented in [22], where the accumulated echogram of a multipath delayed signal is constructed. Stemming from this idea, [23], [24] demonstrated how CIR measurements can be utilized to create a positioning infrastructure. Another study mentioned in [25], employed CIRs to train a Convolutional Neural Network (CNN) model for estimating target positions, while [26] performed a geometrical mapping of the CIRs to reveal reflection sources and derive the occupancy of passengers in the aeronautic field, thus building an IoT network bringing significant operational potentials, such as dynamic control of passenger boarding or disembarkation sequences under pandemic restrictions.

Building upon [24], the contributions of this paper are threefold: i) A comparison between the previous generation of the QORVO UWB module and the newly released generation for radar applications to address the lack of information in the existing literature and contribute to the advancement and optimization of UWB radar systems; ii) A weighting function is introduced to enhance the estimation of the time location of MPCs scattered from the target; iii) An IoT architecture to efficiently handle and organize data for the selected UWB modules.

The rest of the paper is organized as follows: Section II presents the algorithm and the weighting function to estimate the time location of MPCs scattered from the target. The hardware involved in the experiments and preliminary results are described in Section III. Section IV concludes this work with final remarks and possible improvements.

II. METHODOLOGY

The UWB Standard IEEE 802.15.4a [27] utilizes a radio signal composed of a sequence of short pulses, where the signal's bandwidth determines the pulse duration. Upon receiving the preamble of a packet, the system accumulates the symbols, reconstructing the power envelope of the received signal. The data stored in the accumulator serves two primary purposes: calculating timestamps and analyzing

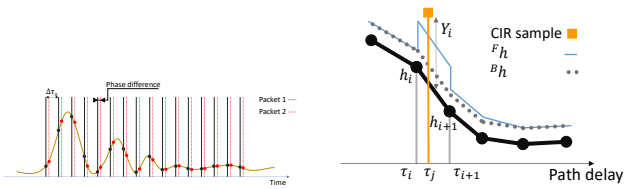

Fig. 1. In (a): CIR obtained by a single receiver, with MPCs labeled as $(\tau_0, \ldots, \tau_n)$. Sampling points are indicated by a black-solid line for received packet 1 and a red-dashed line for the successively received packet; in (b): magnification of a region that shows the piecewise parametrization for the variance metric.

the CIR, compared to the transmitted signal in the time domain. The selected UWB module provides CIR measurements with a resolution of $\Delta\tau_s = 1/(2B_s)$, where $B_s = 499.2$ MHz is the signal bandwidth. It also estimates the time delay of the first path (i.e., the time delay between transmitter and receiver), denoted as τ_{FP}, within each CIR measurement with a resolution of $\Delta\tau_s/64$. In the time domain, the range resolution $R = \frac{c}{2B_s}$ determines the ability to distinguish between targets and depends on the signal bandwidth, resulting in $R = 0.3$ m or $\Delta\tau_s = 1.0016$ ns in the time domain [28].

A. Channel Impulse Response Reconstruction

Radio signals exhibit various propagation phenomena, such as signal reflection, diffraction, and scattering, which affect their transmission. The resulting signal $y(t)$ is represented by the convolution of the CIR $h(t)$ with the input signal $s(t)$ corrupted by a Gaussian white noise process $\varepsilon(t)$, which follows a normal distribution $\varepsilon(t) \sim \mathcal{N}(0, \sigma^2)$, i.e. $y(t) = h(t) * s(t) + \varepsilon(t)$. The temporal behavior of the communication channel is described by the CIR $h(t) = \sum_{n=0}^{N} a_n \delta(t - \tau_n)$, that is a series of N shifted, attenuated, and overlapped UWB pulses $\delta(t - \tau_n)$, where a_n, τ_n represent the amplitude and path delay of n-th MPC respectively and $\delta(\cdot)$ the Dirac delta function. The perfect periodic auto-correlation property of the preamble sequences allows the receiver to accumulate repeated preambles and accurately determine the channel impulse response between the transmitter and receiver [22].

As depicted in Figure 1-(a), in a stable environment, the complex envelope of the received signal (i.e. $h(t)$) remains constant but sampled at different time instants [22]. Consequently, once the initial CIR measurement is obtained, the signal can be discretized up to $B = 64$ bins based on the available timestamping resolution. By aligning subsequent CIRs measurements relative to the time delay of the first path τ_{FP}, each sample within the CIR can be assigned to the appropriate bin, thus acquiring B times more samples and reaching a sub-nanosecond scale.

To compute the time delay τ_{MPC} of the MPC component scattered from the moving target, the algorithm track changes in the CIR variance that is represented as a piecewise constant function with coefficients h_l that are time-updated as

$$ {}^{F}h_l^{(k+1)} = {}^{F}h_l^{(k)} + {}^{F}\beta(|Y_i| - {}^{F}h_l^{(k)}), \tag{1} $$

where $l \in \{0, 1, \ldots, B-2\}$ is such that $\tau_l \leq \tau_j \leq \tau_{l+1}$, ${}^{F}\beta \geq 1$ is a constant scalar sensitivity factor, $|Y_i|$ is the innovation (see Figure 1-(b)) and the superscripts ${}^{F}\cdot$ and $\cdot^{(k)}$ stands for the foreground and time instant. The background variation coefficients ${}^{B}h_l$ are updated using (1) as well. During the initialization phase, the parameter ${}^{B}\beta$ equals ${}^{F}\beta$ to expedite the convergence time for building the background model. Once the background model is reconstructed, the parameter ${}^{B}\beta$ is adjusted to be much smaller than ${}^{F}\beta$. By computing the difference metric $s_l = {}^{F}h_l - {}^{B}\beta {}^{B}h_l$, it is possible to identify segments in the CIR that exhibit higher-than-usual variances within the intervals $\tau_l \leq \tau \leq \tau_{l+1}$, where l is chosen such that $s \geq 0$. Denoting with s_i the i-th sample of the difference metric, its value is normalized by the maximum value of the CIR s_{max} (given by the direct path, i.e., the background), by the number W of consecutive values of $s_j \geq s_i$ (a larger window size W implies the presence of multiple unaccounted multipath generated by the target) and by the ratio between the peak value s_{peak} (occurring when an object enters the scene and creates direct multipath) and s_{max}, i.e.,

$$ w(\tau_T) = W \frac{s_i}{s_{max}} \frac{s_{peak}}{s_{max}}. \tag{2} $$

This difference is related to the time difference between the time delay of the first path and the time delay of the detected MPC τ_{MPC}, i.e., $\tau_T = \tau_{FP} - \tau_{MPC}$, which identifies the target's time of flight, as reported in Figure 2.

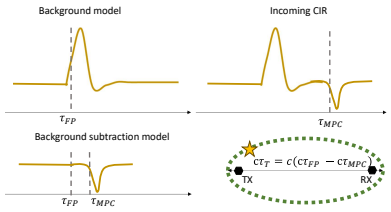

Fig. 2. Graphical representation of the τ_T calculation.

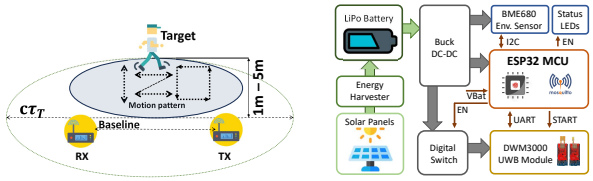

Fig. 3. In (a) experimental setup. A single couple Tx-Rx oriented in the same direction. The receiver analyses CIR to identify the time delay of the target and computes the distance. The target performs various motion patterns within a range of 1-5 m. In (b) radar node prototype.

III. RESULTS

To evaluate the effectiveness of our method, we designed an experimental setup consisting of a single transmitter-receiver pair aligned in the same direction, as depicted in Figure 3-(a). Both the UWB transceivers were configured to sample the surrounding environment at a frequency of approximately 125 Hz.

A. Hardware

The DWM3120 is a second-generation, fully integrated UWB transceiver developed by Qorvo as part of their DW3000 family. It follows the IEEE *802.15.4z* and has the new communication channel 9, operating at a carrier frequency of 7987.2 MHz. Moreover, it is optimized for low-power battery-operated operation, making it suitable for a wide range of mobile, consumer, and industrial applications. To ensure smooth integration into networks, we have developed a prototype whose hardware architecture enables seamless connectivity as depicted in Figure 3-(b). The prototype is endowed with a *Espressif ESP32* microcontroller, a cost-effective and energy-efficient device that comes with built-in WiFi and Bluetooth functionalities; a *TP4056* handling the charge of the batteries; a 3.7 V 1900 mAh LiPo battery; two 5V 1W photovoltaic panels.

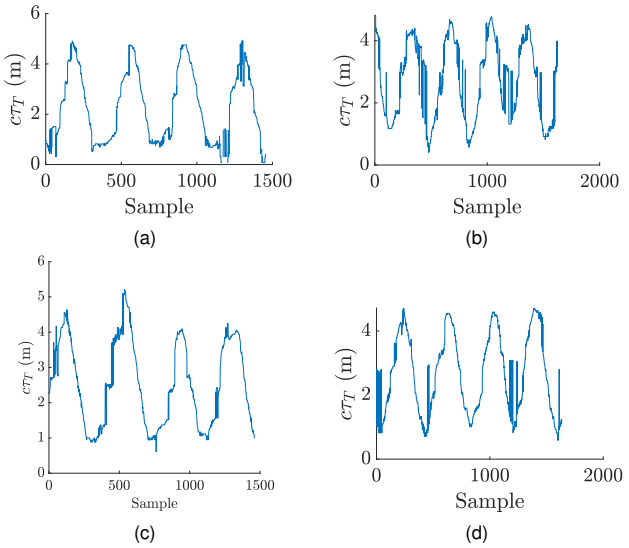

Fig. 4. Bistatic radar for the "Z" shaped motion pattern of Figure 3-(a) with channel 9. (a,c) baseline 2.3 m, (b,d) baseline 4.3 m. (a,b) Tx power level 28.6 dBm/MHz, (c,d) low Tx power level 24.6 dBm/MHz.

B. Preliminary experimental results

The experiments consider four baselines $bl = (1.3, 2.3, 3.3, 4.3)$ m between the transmitter and the receiver, the communication channel 5 and 9, and two transmission power levels 28.6 dBm/MHz and 24.6 dBm/MHz, while various motion patterns are considered, as depicted in Figure 3-(a). The experiments presented in Figure 4 report the results obtained from conducting experiments with channel 9 using both transmission power levels and two different baselines while performing a "Z"-shaped pattern. Based on these preliminary results shown in Figure 4, the choice of the baseline impacts the target distance estimation. Note that for smaller baseline values, the distance estimation significantly deteriorates. We have determined the optimal baseline for our experimental setup through these experiments. This baseline will serve as the reference for comparing and evaluating the performance with channel 5, now. The evaluation is done in a structured indoor environment by using 8 Qualisys Arqus A9 high-performance cameras[1]. Figure 5-(a) illustrates the comparison between the UWB and MoCap traces, while Figure 5-(b) displays the histogram representing the error. Note that the point tracked with motion capture does not align with the virtual point tracked by the UWB radar (i.e., the human body). Consequently, this discrepancy introduces a systematic error in the evaluation, which can be quantified to be approximately 10 cm. For the remaining experiments, raw traces are depicted to provide a comprehensive overview of the experiment's dynamics. A qualitative comparison confirms the improved estimation on channel 9, showing a more stable signal. Channel 5 produces the worst outcomes compared to channel 9, primarily because channel 9 is less susceptible to RF noise in the indoor environment (e.g., WiFi), owing to its higher center frequency. Better results are achieved when the default power transmission (i.e., 24.6 dBm/MHz) is utilized. The increase in transmission power amplifies the amplitude of the noise, leading to more significant fluctuations in the estimated τ_T value. It is important to note that these fluctuations are not solely caused by the estimator but also arise from the variability in timestamping due to internal circuitry sources and the outcome of the leading edge

[1]https://www.qualisys.com/cameras/arqus/#!#tech-specs

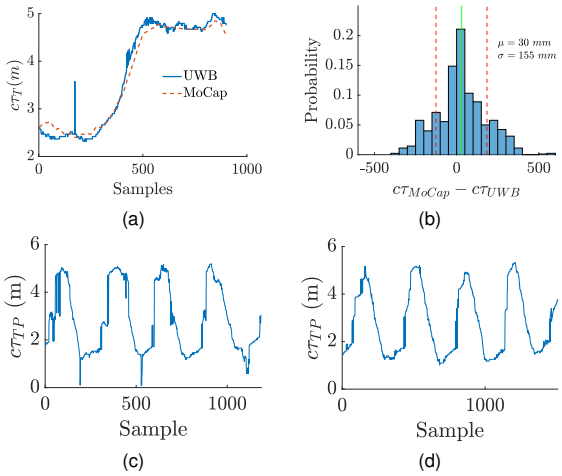

Fig. 5. (a,b) Channel 9 and baseline 4.3 m Square motion pattern of Figure 3-(a): (a) comparison between MoCap and UWB; (b) Histogram of the error. (c,d) UWB radar traces (collected simultaneously) with baseline 2.3 m and back and forth motion pattern of Figure 3-(a): (c) channel 5 (d) channel 9, power transmission level 24.6 dBm/MHz.

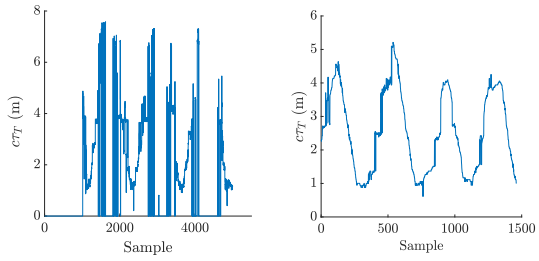

Fig. 6. In (a), the estimated distance using the standard windowing approach on the old generation of UWB devices using channel 5. In (b), the new UWB generation devices using channel 9. Transmission power 24.6 dBm/MHz and baseline 2.3 m

algorithm. Finally, the weighting function (2) greatly enhances the stability and reliability of target distance estimation as compared to our previous work [24] (see Figure 6).

IV. CONCLUSION

Device-Free localization holds great potential for facilitating the widespread adoption of indoor localization infrastructures. However, existing solutions often suffer from limitations such as reliance on custom or expensive hardware, which hinders their scalability. This study evaluates the advancements offered by a compact and cost-effective radar node system that utilizes DW3000 UWB transceivers for device-free positioning to address these challenges. The results obtained from the experiments demonstrate the effectiveness of the newly developed hardware, particularly in channel 9 with 24.6 dBm/MHz transmission power. The evaluation is conducted using CIR analysis and a bistatic radar configuration. Furthermore, integrating a weighting function has significantly improved the estimation stability and accuracy of τ_T. In future research, we will focus on exploring UWB in multi-target scenarios. In this experimental configuration, we consider the presence of a single moving target. However, the same methodology can be applied to identify multiple τ_T values within the measured CIR. Furthermore, we intend to investigate its innovative use in robotics, where UWB can serve as a Time-of-Flight (ToF) sensor, enabling the development of advanced obstacle avoidance systems.

ACKNOWLEDGMENT

This work was partially supported by the GEMINI ("Green Machine Learning for the IoT") national research project, funded by the Italian Ministry for University and Research (MUR) by the PRIN 2022 programme (Contract 20223M4HZ4).

Moreover, this work was supported by the Italian Ministry for University and Research (MUR) under the program "Dipartimenti di Eccellenza (2023-2027).

Further, this work is based on and improves the achievements of iNEST (interconnected NordEst innovation Ecosystem, Project ID: ECS00000043) PNRR project (Mission 4.2, Investment 1.5) Spoke 3 "Green and digital transition for advanced manufacturing technology", funded by the European Commission under the NextGeneration EU programme.

REFERENCES

[1] M. Nardello, L. Santoro, F. Pilati, and D. Brunelli, "Preventing covid-19 contagion in industrial environments through anonymous contact tracing," in *2021 IEEE International Workshop on Metrology for Industry 4.0 & IoT (MetroInd4.0&IoT)*, 2021, pp. 99–104.

[2] M. Kolakowski and V. Djaja-Josko, "Tdoa-twr based positioning algorithm for uwb localization system," in *2016 21st International Conference on Microwave, Radar and Wireless Communications (MIKON)*, 2016, pp. 1–4.

[3] J. Ninnemann, P. Schwarzbach, A. Jung, and O. Michler, "Lab-based evaluation of device-free passive localization using multipath channel information," *Sensors*, vol. 21, no. 7, 2021.

[4] L. Santoro, D. Brunelli, and D. Fontanelli, "On-line optimal ranging sensor deployment for robotic exploration," *IEEE Sensors Journal*, vol. 22, no. 6, pp. 5417–5426, 2021.

[5] L. Santoro, M. Nardello, D. Fontanelli, D. Brunelli, and D. Petri, "Scalable centimetric tracking system for team sports," in *2022 IEEE International Workshop on Sport, Technology and Research (STAR)*, 2022, pp. 1–6.

[6] D. Brunelli, E. Farella, D. Giovanelli, B. Milosevic, and I. Minakov, "Design considerations for wireless acquisition of multichannel semg signals in prosthetic hand control," *IEEE Sensors Journal*, vol. 16, no. 23, pp. 8338–8347, 2016.

[7] E. Farella, A. Pieracci, and A. Acquaviva, "Design and implementation of wimoca node for a body area wireless sensor network," in *2005 Systems Communications (ICW'05, ICHSN'05, ICMCS'05, SENET'05)*, 2005, pp. 342–347.

[8] D. Brunelli, E. Farella, L. Rocchi, M. Dozza, L. Chiari, and L. Benini, "Bio-feedback system for rehabilitation based on a wireless body area network," in *Fourth Annual IEEE International Conference on Pervasive Computing and Communications Workshops (PERCOMW'06)*, 2006, pp. 5 pp.–531.

[9] H.-S. Cho, H.-K. Lyu, and Y.-J. Park, "Noninvasive heartbeat extraction from ir uwb radar signals," in *2015 International Conference on Information and Communication Technology Convergence (ICTC)*, 2015, pp. 977–980.

[10] H. Lv, M. Liu, T. Jiao, Y. Zhang, X. Yu, S. Li, X. Jing, and J. Wang, "Multi-target human sensing via uwb bio-radar based on multiple antennas," in *2013 IEEE International Conference of IEEE Region 10 (TENCON 2013)*, 2013, pp. 1–4.

[11] L. Santoro, M. Nardello, D. Brunelli, and D. Fontanelli, "Uwb-based indoor positioning system with infinite scalability," *IEEE Transactions on Instrumentation and Measurement*, pp. 1–1, 2023.

[12] F. Alam, N. Faulkner, and B. Parr, "Device-free localization: A review of non-rf techniques for unobtrusive indoor positioning," *IEEE Internet of Things Journal*, vol. 8, no. 6, pp. 4228–4249, 2020.

[13] Y.-C. Huang, C.-W. Liu, and J.-H. Chuang, "Using fisheye camera for cost-effective multi-view people localization," in *2021 IEEE International Conference on Image Processing (ICIP)*, 2021, pp. 3248–3252.

[14] N. Anjum and A. Cavallaro, "Localization of distributed wireless cameras," in *2009 Third ACM/IEEE International Conference on Distributed Smart Cameras (ICDSC)*, 2009, pp. 1–6.

[15] C.-C. Hsu, H.-C. Chen, and C.-Y. Lai, "An improved ultrasonic-based localization using reflection method," in *2009 International Asia Conference on Informatics in Control, Automation and Robotics*, 2009, pp. 437–440.

[16] M. Alves, R. Coelho, and E. Dranka, "Effective acoustic energy sensing exploitation for target sources localization in urban acoustic scenes," *IEEE Sensors Letters*, vol. 4, no. 2, pp. 1–4, 2020.

[17] A. E. Kosba, A. Saeed, and M. Youssef, "Rasid: A robust wlan device-free passive motion detection system," in *2012 IEEE International Conference on Pervasive Computing and Communications*. IEEE, 2012, pp. 180–189.

[18] S. Denis, B. Bellekens, A. Kaya, R. Berkvens, and M. Weyn, "Large-scale crowd analysis through the use of passive radio sensing networks," *Sensors*, vol. 20, no. 9, p. 2624, 2020.

[19] N. J. Meyerhoff, "Intrusion detection by ultra-wide bandwidth radar," in *2007 IEEE Conference on Technologies for Homeland Security*, 2007, pp. 81–84.

[20] K. Jung, Y. Bang, and S.-M. Hwang, "Study on detection algorithm of live animal in self-bag-drop kiosk in airport using uwb radar," in *2018 19th IEEE/ACIS International Conference on Software Engineering, Artificial Intelligence, Networking and Parallel/Distributed Computing (SNPD)*, 2018, pp. 242–245.

[21] S. Palipana, B. Pietropaoli, and D. Pesch, "Recent advances in rf-based passive device-free localisation for indoor applications," *Ad Hoc Networks*, vol. 64, pp. 80–98, 2017.

[22] A. Moschevikin, E. Tsvetkov, A. Alekseev, and A. Sikora, "Investigations on passive channel impulse response of ultra wide band signals for monitoring and safety applications," in *2016 3rd International Symposium on Wireless Systems within the Conferences on Intelligent Data Acquisition and Advanced Computing Systems (IDAACS-SWS)*, 2016, pp. 97–104.

[23] A. Ledergerber and R. D'Andrea, "A multi-static radar network with ultra-wideband radio-equipped devices," *Sensors (Basel)*, vol. 20, no. 6, mar 2020.

[24] M. Doglioni, L. Santoro, M. Nardello, D. Fontanelli, and D. Brunelli, "Cost-effective bistatic radar with ultrawide-band radio," in *2022 IEEE International Workshop on Metrology for Industry 4.0 & IoT (MetroInd4. 0&IoT)*. IEEE, 2022, pp. 207–211.

[25] C. Li, E. Tanghe, J. Fontaine, L. Martens, J. Romme, G. Singh, E. De Poorter, and W. Joseph, "Multistatic uwb radar-based passive human tracking using cots devices," *IEEE Antennas and Wireless Propagation Letters*, vol. 21, no. 4, pp. 695–699, 2022.

[26] M. Cimdins, S. O. Schmidt, F. John, M. Constapel, and H. Hellbrück, "Ma-rti: Design and evaluation of a real-world multipath-assisted device-free localization system," *Sensors (Basel)*, vol. 23, no. 4, feb 2023.

[27] I. S. Association *et al.*, "Ieee standard for local and metropolitan area networks—part 15.6: Wireless body area networks," *IEEE std*, vol. 802, no. 6, p. 2012, 2012.

[28] J. Kulmer, S. Hinteregger, B. Großwindhager, M. Rath, M. S. Bakr, E. Leitinger, and K. Witrisal, "Using decawave uwb transceivers for high-accuracy multipath-assisted indoor positioning," in *2017 IEEE International Conference on Communications Workshops (ICC Workshops)*, 2017, pp. 1239–1245.